ScieRxiv

NOT PEER-REVIEWED

Original Article

Improved isolation and biomarker measurement in blood-based CNS-originating extracellular vesicles

Gal Bitan[1,2,3*], Ibrar Siddique[1], Yangxia Wang[1], Marie Khijniak[1], Megan Hong[1,2], Patricio Millar Vernetti[4], Horacio Kaufmann[4], Nadia Stefanova[5]

[1]Department of Neurology, David Geffen School of Medicine, University of California, Los Angeles, CA 90095, USA.

[2]Molecular Biology Institute, University of California, Los Angeles, CA 90095, USA.

[3]Brain Research Institute, University of California, Los Angeles, CA 90095, USA.

[4]Department of Neurology, Dysautonomia Center, The Marlene and Paolo Fresco Institute for Parkinson's and Movement Disorders, New York University School of Medicine, New York, NY 10016, USA.

[5]Division of Neurobiology, Department of Neurology, Medical University of Innsbruck, Tyrol 6020, Austria.

***Correspondence to:** Dr. Gal Bitan, Department of Neurology, David Geffen School of Medicine, University of California, Los Angeles, Los Angeles, CA 90095, USA. E-mail: gbitan@mednet.ucla.edu

Received: 24 June 2026 | Approved: 27 July 2026 | Online: 27 July 2026

Abstract

CNS-originating extracellular vesicles (EVs) isolated from plasma or serum are a rich source of biomarkers, offering insight into biochemical processes in the CNS. Such EVs are isolated by immunoprecipitation (IP) using specific cellular markers on their membrane. The marker

and antibody choice affect specificity, as some markers are expressed mainly, but not exclusively, in the target cells. Additionally, different markers of the same cell type may yield distinct biomarker data. In particular, the use of the neuronal marker L1-cell adhesion molecule (L1CAM) for isolation of neuronal EVs has been scrutinized, leading to identification of alternative markers, yet a side-by-side comparison of these markers has not been reported to date. To address this knowledge gap, we compared the yield and purity of EVs IP'd using L1CAM to three recently proposed markers, GAP-43, NLGN3, and ATP1A3 to determine whether any of the markers may be superior to others. An additional practical challenge in studying biomarkers in EVs from different cell types is the limited sample volume. To tackle this issue, we tested isolation of EVs originating in different cell types from the same sample aliquot comparing the yield to isolating a single EV type. Our marker comparison showed that NLGN3 provided higher nEV yield and specificity to CNS neurons. Isolating nEVs and oligodendroglial EVs from the same sample is feasible with minimal yield loss if nEVs are isolated first. Finally, we demonstrate further improved utilization of small samples volumes for the Parkinson's disease biomarkers α-synuclein and pS129-α-synuclein using a duplex electrochemiluminescence immunoassay.

Keywords: Cell-specific extracellular vesicles, immunoprecipitation, cell-specific markers, technical improvement, α-synuclein.

INTRODUCTION

Extracellular vesicles (EVs) are a diverse group of lipid bilayer-enclosed nanoparticles that vary in size, function, and biomolecular cargo[1]. Common types of EVs are microvesicles, which evaginate directly from the plasma membrane and exosomes, which form upon the fusion of multivesicular bodies generated in the endosomal pathway with the plasma membrane, leading to the release of their intraluminal vesicles to the extracellular space, at which point these vesicles are called exosomes[2]. Biomolecules carried by the EVs include lipids, proteins, mRNA, microRNA, DNA, metabolites, and in particularly large EVs, such as exophers, even whole organelles[3,4]. Once secreted, the EVs may be taken up by other cells, serving in intercellular communication[5], and under stress conditions, also may assist in removal or unwanted cellular material, such as abnormal protein aggregates[6,7].

EVs have been detected in many body fluids, such as blood, cerebrospinal fluid (CSF), urine, saliva, and breast milk[8]. Their widespread presence in various biofluids and the protection they provide their cargo from catabolic enzymes allow the EV content to reflect the origin and functional state of their parent cells[9], making them an attractive source of biomarkers, especially for difficult-to-access organs, such as the CNS[10]. In recent years, CNS-originating EVs isolated primarily from blood products, plasma or serum, particularly neuronal EVs (nEVs), have been used increasingly as a minimally invasive liquid biopsy for different neurodegenerative diseases, including Alzheimer's disease (AD)[11-13], Parkinson's disease (PD)[14-16], Prion disease[17], amyotrophic lateral sclerosis[18,19], and others[20,21].

Studies of biomarkers in CNS-originating EVs commonly utilize immunoaffinity pulldown techniques that target proteins expressed selectively by the originating cells and present on the surface of the released EVs. The L1 neuronal cell adhesion molecule (L1CAM) has been used most frequently for isolation of nEVs following the pioneering work of the Zhang[14] and Goetzl/Kapogiannis[11] groups. L1CAM typically is expressed as a single-pass transmembrane protein containing immunoglobulin- and fibronectin-like repeat domains in the extracellular, N-terminal portion, and a cytoplasmic C-terminal tail that plays a role in intracellular signaling[22]. However, data in the Protein Atlas (www.proteinatlas.org) indicate that although L1CAM is enriched primarily in neurons, it is expressed also by other cells, particularly distal renal tubules and melanocytes. In addition, isoforms of L1CAM that are not membrane-associated are abundant in the blood[23], raising the question whether LICAM can be used to isolate nEVs from bodily fluids efficiently[24]. This concern has prompted active discussion in the field about the use of L1CAM for isolation of nEV[25] and subsequent studies, including by our group[26], demonstrating effective enrichment of nEVs using this marker. An elegant study by Nogueras-Ortiz *et al.* not only demonstrated that L1CAM was enriched in nEVs compared to EVs isolated from other cells but also revealed that free-floating L1CAM did not bind to the surface of EVs[27].

Nonetheless, in search of other neuron-specific markers for isolation of nEVs, Eitan *et al.* have used growth-associated protein 43 (GAP-43) together with neuroligin 3 (NLGN3) for

immunoprecipitating nEVs and demonstrated their utility for analysis of AD biomarkers[28]. Separately, You *et al.* have demonstrated that the α3 subunit of the sodium-potassium pump (Na^+/K^+ ATPase, ATP1A3) could be used as a specific marker allowing immunoprecipitation (IP) of nEVs[29], comparing this new marker with L1CAM and another marker used in earlier studies, NCAM[11]. Super-resolution imaging of EVs stained with fluorescently labeled antibodies against the EV markers CD9/CD81/CD63 suggested that ATP1A3 provided higher selectivity for neuronal EVs than L1CAM or NCAM. However, to our knowledge, a systematic comparison among these new markers, GAP-43, NLGN3, and ATP1A3 has not been done to date.

Though nEVs have been the most commonly used type of CNS-originating EVs in biomarker studies, astroglial[30-32] and oligodendroglial[26,33,34] EVs (aEVs and oEVs, respectively) also have been used for this purpose. For example, a previous study by our group has shown that in some cases, analysis of a biomarker in EVs originating in different cells could be the key to reaching high sensitivity and specificity. Thus, whereas measurement of α-synuclein (α-syn) concentration in nEVs or oEVs separated between PD and the related synucleinopathy, multiple system atrophy (MSA) in a receiver operating characteristic (ROC) analysis with an area under the curve (AUC) = 0.769, and 0.867, respectively, the ratio between the oEV and nEV concentrations improved the separation yielding AUC = 0.913. However, procuring a sufficient serum or plasma volume from patients for isolation of two or more EV types can be challenging, especially when the samples are obtained from biorepositories serving the broad research community. A possible solution is orthogonal isolation of EVs by IP using different antibodies sequentially from the same sample [Figure 1]. This approach has been demonstrated recently in a small proteomics study for which at least one mL of serum was available for each sample[35] and there was no attempt to evaluate the potential loss of yield or whether the order of IP reactions impacted the yield.

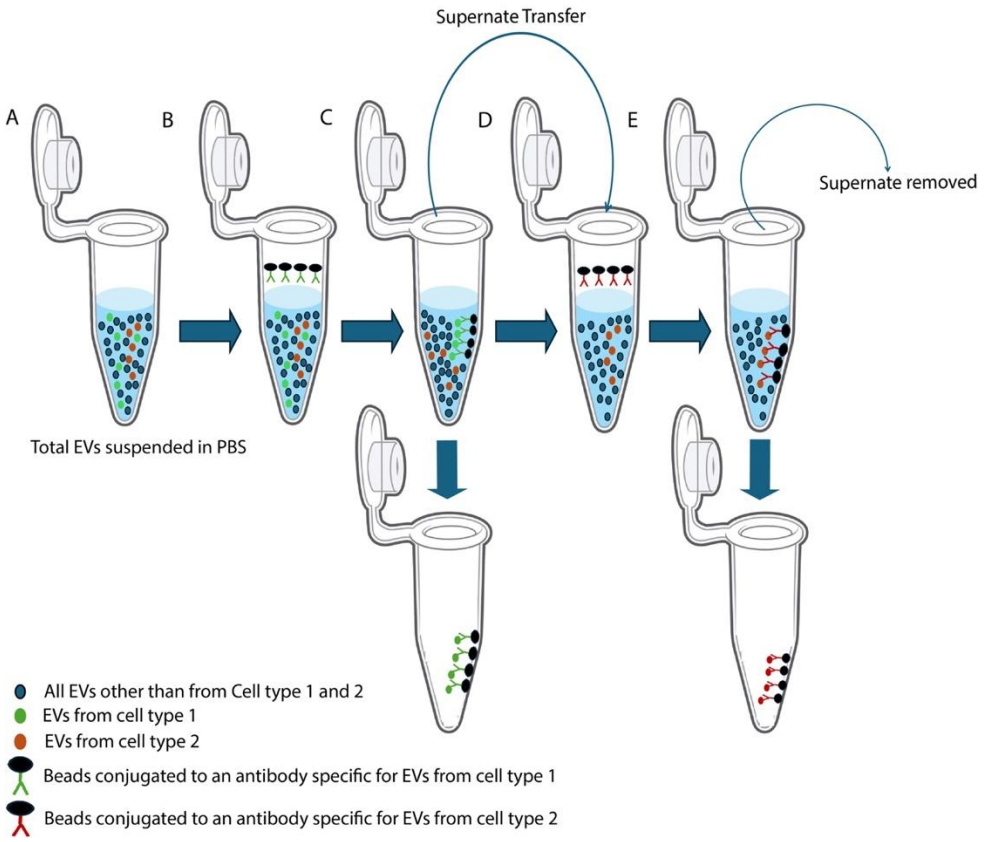

Figure 1. Illustration of serial immuno-isolation of nEVs and oEVs from the same sample. A) Total extracellular vesicles (EVs) precipitated from a biofluid sample and resuspended in PBS; B) To isolate cell-specific EVs, magnetic beads conjugated to an antibody specific for a surface marker of the first cell type are added to the EV suspension and incubated at 4 °C with continuous rotation; C) EVs of the first cell type are isolated using a magnet, leaving all other EVs in the supernate; D) The supernate is transferred to a new vial, and magnetic beads conjugated to an antibody specific for a surface marker of EVs from a second cell type are added and incubated with the remaining EVs; E) EVs from the second cell type are isolated using a magnet. The Eppendorf tubes shown in the illustration were created using BioRender (BioRender.com).

To address these current knowledge gaps, here, we compared the yield and specificity of the neuronal markers L1CAM, GAP-43, NLGNs, and ATP1A3, and tested the feasibility of isolating nEVs and oEVs sequentially from the same sample. Our data suggest that NLGN3 is superior to the other markers for isolation of nEVs, that sequential isolation of EVs from

different cell types is feasible, and that the order of isolation is important for maximizing the yield.

MATERIALS AND METHODS

EV precipitation from serum

Total EV precipitation from human pooled serum (Innovative Research, Novi, MI) was done using the ExoQuick kit (System Biosciences, Palo Alto, CA) as described previously[26,36]. All the markers of EVs or different cell types or tissues were analyzed in the EV pellet and the EV-depleted serum.

IP of neuronal or oligodendroglial EVs

nEVs were IP'd essentially as described previously[26]. In addition to using beads conjugated to an anti-L1CAM antibody, we also conjugated beads to antibodies against GAP-43, NLGN3, or ATP1A3 [Table 1]. oEVs were IP'd using an anti-MOG antibody as described previously[26]. Briefly, 2 µg of antibody were conjugated to 1 mg of M-270 epoxy Dynabeads™ (Thermo Fisher Scientific, Canoga Park, CA) using a Dynabeads™ Antibody Coupling Kit (Life Technologies, Carlsbad, CA) overnight at 37 °C following the manufacturer's instructions. The antibody-coated beads were mixed gently with the resuspended EVs in phosphate-buffered saline (PBS, diluted from 10X PBS, Thermo Fisher Scientific), pH 7.4, containing 1% (w/v) bovine serum albumin (BSA, Sigma-Aldrich, St. Louis, MO) and a protease and phosphatase inhibitor cocktail (PPi, Sigma-Aldrich) and incubated overnight at 4 °C with gentle rotation. The bead-attached EVs were then washed using 0.1% (w/v) BSA in PBS, pH 7.4, and lysed by incubation in 20 µL of RIPA buffer for 1 h at 4 °C. For characterization using NTA or ExoView, the EVs were released by incubation in a glycine-HCl buffer, pH = 2, for 10 min at room temperature, following which the solution was neutralized using Tris-HCl, pH = 8.

Table 1. Antibodies used in this study.

Antigen/Antibody	Source/Catalog no.
L1CAM	Santa Cruz Biotechnology/SC33686
GAP-43	Thermo Scientific/33-5000

NLGN3	Santa Cruz Biotechnology/SC137052
ATP1A3	Invitrogen/ANP-003
MOG	Santa Cruz Biotechnology/SC376138
Syntenin-1	Cell Signaling Technology/#27964
pS129 α-Syn/EP1536Y	Abcam/Ab51253
HRP-Tag Anti-Rabbit	Santa Cruz Biotechnology/SC2357
HRP-Tag Anti-Mouse	Santa Cruz Biotechnology/SC358914

Nanoparticle tracking analysis (NTA)

The size distribution and concentration of the isolated EVs after immunoprecipitation using the anti-NLGN3 antibody and glycine-buffer release were assessed by NTA using a NanoSight NS300 instrument equipped with a 532-nm laser (Malvern Panalytical, UK) and analyzed using NanoSight NTA software version 3.4. Samples were diluted 1:500 in particle-free PBS to achieve an optimal concentration of 10-100 particles per frame. Data collection included five 60-second videos at a controlled temperature of 25 °C. The hydrodynamic diameter (both mean and mode) and particle concentration were determined by averaging the results of these five recordings.

ExoView

EV surface marker profiling and colocalization analysis was carried out using the ExoView R100 platform (NanoView Biosciences). Samples were diluted in the provided incubation buffer and applied to ExoView Tetraspanin chips coated with capture antibodies for CD9, CD63, and CD81, along with murine IgG1 (MIgG1, Clone MOPC-21) as a non-specific binding control. After an overnight incubation at room temperature, the chips were washed and then incubated for 1 h with a fluorescent detection antibody cocktail targeting CD9 (Blue), CD63 (Red), or CD81 (Green). After automated washing and drying, the chips were imaged using the ExoView R100 imager. Data analysis was performed using ExoView Analyzer software version 3.2. Particle size was measured by interferometry (SP-IRIS) and marker colocalization was evaluated using predefined fluorescence thresholds (400 a.u. for CD9, 350 a.u. for CD63 and CD81). The total number of particles and the percentage of

vesicles positive for multiple markers (breakdown analysis) were determined across three independent technical replicates per chip.

ELISA

ELISA kits were used to measure the human proteins microtubule associated protein-2 (MAP-2), apolipoprotein B (ApoB), 2',3'-cyclic nucleotide 3'-phosphodiesterase (CNPase), cytochrome C (CytC), epithelial cadherin (E-cadherin), glycoprotein A-33 (GPA33), glutamate receptor, ionotropic, *N*-methyl D-aspartate 2B (GRIN2B), prominin-2, and creatine kinase, M-type (CKM) [Table 2] according to the manufacturer's instructions for each kit. Briefly and generally, standards, blanks, or samples were added to each well and incubated for 90 min at 37 °C. The liquid was aspirated, followed by incubation with biotinylated detection antibodies for 1 h at 37 °C with gentle agitation. The liquid was then aspirated again, and the plate was washed thrice using the supplied wash buffer. Then, an HRP-conjugated secondary antibodies were added and incubated for 30 min at 37 °C. The liquid was aspirated once more, and the plate was washed five times. 3,3',5,5'-tetramethylbenzidine substrate was added to each well and incubated for 15 min at 37 °C. Finally, a stop solution was added, mixed gently, and the plate was read using a BioTek Synergy HTX plate reader (Agilent, Santa Clara, CA) at 450 nm.

Table 2. ELISA and electrochemiluminescence immunoassay (ECLIA) kits used.

Type of measurement	Antigen	LLoD[1] (pg/mL)	LLoQ[1] (pg/mL)	ULoQ[1] (pg/mL)	Source
ELISA	MAP-2	17.5	32.5	4,000	LSBio
	GRIN2B	31	31	20,000	LSBio
	GPA33	37.5	62.5	40,000	LSBio
	CytC	15	31.2	2,000	LSBio
	Apolipoprotein B	46.9	78.1	5,000	LSBio
	E-Cadherin	94	188	12,000	Antibodies.com

	CNPase	188	313	20,000	LSBio
	Prominin-2	1	15	240	MyBioSource.com
	CKM	18.9	62.5	4,000	Abcam
ECLIA	α-Synuclein	0.9	8	6,800	MSD
	CD81	N/A	N/A	N/A	MSD

[1]Abbreviations: LLoD – lower limit of detection, LLoQ – lower limit of quantitation, ULoQ – upper limit of quantitation.

Electrochemiluminescense immunoassay (ECLIA) measurement of α-syn

ECLIA is an antibody-based detection technique that uses electrochemically triggered light emission from a labeled detection antibody to measure analytes with high sensitivity and a wide dynamic range[37]. The concentration of α-Syn in nEVs was measured using the U-PLEX Human α-Synuclein kit (Meso Scale Diagnostics (MSD), Rockville, MD) according to the manufacturer's instructions, as described previously[36]. Briefly, a biotinylated anti-human α-syn capture antibody was added to small-spot streptavidin-coated wells and incubated at room temperature for 1 h. After washing, samples and calibration standards were added along with a Sulfo-TAG-conjugated anti-human α-syn detection antibody and incubated at room temperature for 2 h. Following washing, a read buffer was added, and the plates were read using a 1300 Meso® QuickPlex SQ 120 MM instrument (MSD). The data were analyzed using Discovery Workbench 4.0 software.

Duplex measurement of α-syn and pS129-α-syn

We used antibody EP1536Y (Abcam, Waltham, MA), biotinylated using a protein biotinylating kit (Thermo Fisher Scientific, Canoga Park, CA), as a capture antibody for pS129-α-syn, and a biotinylated antibody provided in the U-PLEX Human α-Synuclein kit to capture total α-syn. Purified semisynthetic pS129-α-syn (Proteos, Kalamazoo, MI) was used as the standard. The anti-pS129-α-syn antibody was coated on spot-1 of an MSD assay development plate, and the anti-α-syn antibody was coated on spot-10, following the manufacturer's protocol with some modifications. Briefly, 1 µg of antibody EP1536Y was added to 30 µL of Linker 1, and the volume was brought to 50 µL with PBS. Total α-syn antibody was diluted to the working concentration in a 50 µL solution comprising 30 µL of

Linker 1 and 20 µL PBS. The mixtures were incubated at room temperature for 30 min. Then, 20 µL of stop solution was added and incubated at room temperature for an additional 30 min. The antibody linker complex was mixed and diluted using the stop solution to a 1 × concentration. 50 µL of coating solution was added to each well, and the plate was shaken at 700 rpm at room temperature for 1 h. The plate was washed thrice with PBS-T, and 25 µL of samples or standards (for both analytes), and 25 µL detection antibody were added to each well. The samples contained a brain lysate of a six-month-old, male, homozygous, transgenic PLP-α-syn mouse (MGI: 3604008) overexpressing human α-syn under the PLP-promoter[38] and nEVs isolated from the serum of a 56-year-old patient with MSA-C used in a previous study[26]. The plate was shaken at 700 rpm at room temperature for 2 h, washed thrice with PBS-T, then 150 µL of read buffer was added, and the plate was read using a MESO QuickPlex SQ 120MM instrument. The data were analyzed using Discovery Workbench 4.0 software.

ECLIA measurement of CD81

CD81 concentrations were measured using an MSD R-Plex Human CD-81 kit according to the manufacturer's protocol. Briefly, a biotinylated anti-human CD81 antibody was attached to the streptavidin-coated plate. The plate was washed, then samples and standards were added and incubated at room temperature for 1 h. Following additional washing, the detection antibody was incubated with the samples and after final washing, read buffer was added and the values were read using a MESO QuickPlex SQ 120MM instrument. The data were analyzed using Discovery Workbench 4.0 software.

Immunoblotting

100 µg of total protein from EV-lysates or EV-depleted serum were mixed with sample buffer containing 100 mM dithiothreitol (GenScript, Piscataway, NJ) and heated at 95 °C for 10 min. The mixtures were fractionated using SurePAGE 4-20% gradient bis-Tris gels (GenScript). Then, the proteins were transferred to polyvinylidene fluoride (PVDF) membranes (Thermo Fisher Scientific) for 1 h at 25 V on ice using XCell II blot modules (Invitrogen). The membranes were blocked with 5% (w/v) nonfat dry milk (Thermo Fisher Scientific) in TBS-T (blocking solution) for 1 h at room temperature and then incubated with

the appropriate antibodies [Table 1] at a 1:1,000 dilution in blocking solution overnight at 4 °C with gentle agitation. The membranes were washed thrice in TBS-T, incubated with HRP-conjugated anti-rabbit or anti-mouse secondary antibodies, as appropriate, at a 1:10,000 dilution in blocking solution for 1 h at room temperature, and developed using SuperSignal West Pico PLUS chemiluminescent substrate (Life Technologies). Protein bands were visualized using a c300 gel imager (Azure Biosystems, Dublin, CA).

Protein assay

Protein concentration was estimated using a bicinchoninic-acid (BCA) assay kit (Thermo Scientific) following the manufacturer's protocol.

Statistical analysis

Statistical analyses were performed using Prism 11.0 (GraphPad, La Jolla, CA). Data comparisons were conducted using a *t*-test, one-way ANOVA, or two-way ANOVA, as appropriate. Sample concentrations below the LLoD were imputed as the minimum value divided by 2.

RESULTS

EV characterization

To determine how GAP-43, NLGN3, and ATP1A3 compared to L1CAM and to each other in terms of efficiency and specificity of immunoprecipitating nEVs, we conjugated an antibody against each marker to magnetic Dynabeads™, mixed the antibody-conjugated beads with EVs isolated from commercial human serum, washed and then lysed the EVs, and measured the concentration of different markers in them. In parallel, we used myelin oligodendrocyte glycoprotein (MOG)—a brain protein that plays a major role in the formation and maintenance of the myelin sheath and is found primarily in oligodendrocytes[39]—for IP of oEVs. To validate successful isolation of EVs and test whether the process yielded comparable EV amounts, we used immunoblotting for the EV marker syntenin-1, followed by densitometric analysis. Syntenin-1 migrated mainly as a 32-kDa band as expected, along with three minor higher-molecular-weight bands, likely representing ubiquitinated and/or glycosylated forms[40], and two minor lower-molecular-

weight bands probably representing degradation products. The analysis supported isolation of roughly equal amounts of EVs by each surface marker within experimental variability [Figure 2A, B].

To validate the presence of additional EV markers, we used the imaging platform ExoView. We captured the preparations using antibodies against the tetraspanins CD9, CD63, or CD81, and then detected the presence of each marker in each EV population. The analysis confirmed the presence of the three tetraspanins and showed that CD9 was the most abundant among them, yielding 2,607 ± 150 total particles in 20 µL of solution. In comparison, the CD63 probe captured 526 ± 50 particles in the same volume and the number of particles captured by the CD81 probe, 260 ± 40, was similar to that captured by the control mouse IgG1 [Figure 2C, D]. Colocalization analysis showed that 86% of the EVs captured by the CD9 antibody were positive for CD9, 35% showed colocalization of CD9 and CD63, 7% showed colocalization of CD9 and CD81, and 8% were triple-positive for all three tetraspanins. The small population captured by the CD63 or CD81 antibodies showed different populations of single, double, and triple labeling for the three tetraspanins [Figure 2E].

To further characterize the nEVs, we released those IP'd using beads conjugated to an anti-NLGN3 antibody, as representatives of immunocaptured EVs, and measured their concentration and hydrodynamic diameter using NTA. The concentration found was $1.5 \times 10^{11} \pm 1 \times 10^{10}$ particles/mL, indicating a high yield following release. The average particle diameter was 130 ± 4 nm, with a range of 105 ± 6 nm. The particle size distribution showed a D10 of 83 nm (i.e., 10% of particles are below 83 nm), a D50 of 122 nm, and a D90 of 186 nm, suggesting that the captured EVs were primarily small EV consistent with the exosome size range [Figure 2F].

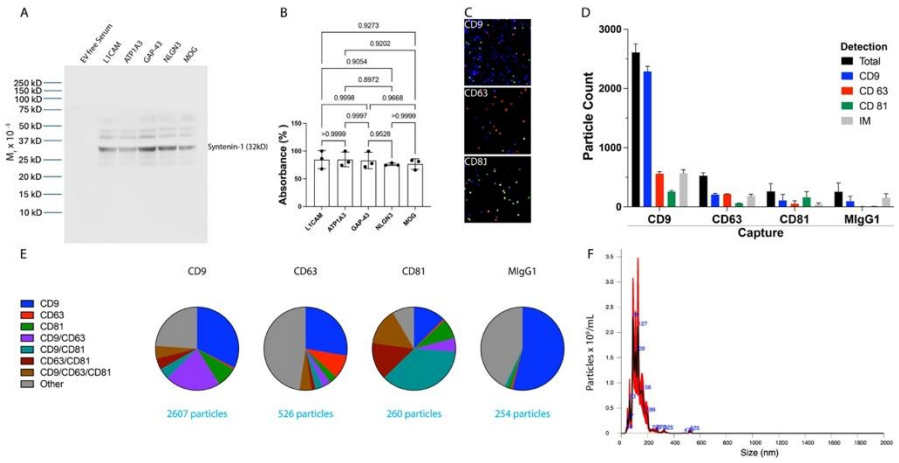

Figure 2. Biochemical and biophysical Characterization of nEVs. A) A representative immunoblot of syntenin-1 in nEVs isolated using antibodies specific for L1CAM, ATP1A3, GAP-43, NLGN3, or MOG; B) Densitometric analysis of syntenin-1 immunoblots (N = 3); P-values were calculated using a one-way ANOVA with Tukey correction for multiple comparisons; C) Representative ExoView fluorescence images demonstrating binding of EV to chips coated with antibodies against CD9, CD63, or CD81; D) Total particle counts of nEVs captured on ExoView chips using anti-CD9, anti-CD63, anti-CD81, or a negative-control mouse IgG1. Interferometric measurements (IM, grey bars) indicate total physical capture whereas colored bars represent fluorescent subpopulations positive for CD9, CD63; or CD81; E) Breakdown analysis of vesicle subpopulations across the three capture probes; F) A representative size distribution profile of nEVs released from Dynabeads™ conjugated to an anti-NLGN3 antibody, obtained using NanoSight NS300. The black line shows the mean of five independent video captures, each represented by the red lines.

Side-by-side comparison of nEV IP using different neuronal markers

To compare the specificity and yield among the four surface markers used for IP of nEVs, following the IP using each marker, we lysed the EVs and measured several markers in them: To validate the EVs neuronal origin an compare their relative yield, we measured the neuronal markers MAP-2 and GRIN2B. MAP-2 plays a critical role in stabilizing microtubules and promoting the structure and function of dendrites, making it a widely used marker for identifying neuronal cells, as it is generally absent in glia[41]. GRIN2B is a subunit of the *N*-methyl-D-aspartate receptor, primarily involved in excitatory synaptic transmission, synaptic plasticity, and neurodevelopment. It is found similarly predominantly in neurons[42].

As a negative control for nEVs, and to validate the origin of oEV IP'd using an anti-MOG antibody, we measured the concentration of the oligodendrocyte marker 2′,3′-cyclic nucleotide 3′-phosphodiesterase (CNPase)[43]. Additionally, we measured cytochrome C, which is typically absent, or present at low levels, in EV[44,45], as a negative control; prominin-2 and E-cadherin, as markers of multiple peripheral tissues, including renal tubules in which L1CAM is thought to be enriched; GPA33, a protein enriched in multiple gastrointestinal (GI)-tract cells, another tissue in which L1CAM is expressed; and CKM as a marker of muscle cells, because ATP1A3 has been reported to be expressed in the heart[46,47]. All the markers were measured using commercial ELISA kits [Table 2], and the measurements were normalized by loading an equal amount of total protein, in most cases 10 µg, from each lysate in each well. In addition, 25 µL of unfractionated serum, not normalized by its total protein concentration, was used as a positive control simply to validate that the assay worked as expected in each case.

The four neuronal markers used for IP yielded similar MAP-2 concentrations, yet the yield obtained using the anti-NLGN3 antibody was 14-19% higher than using the other markers [Figure 3A, Table 3]. Similarly, IP using NLGN3 as the target marker resulted in 17-27% higher GRIN2B concentrations compared to the other markers [Figure 3B, Table 3]. IP using an anti-MOG antibody yielded substantially lower concentrations of MAP-2 or GRIN2B, as expected [Figures 3A, B, Table 3]. Conversely, the concentration levels of CNPase were > 10-times higher in the oEVs IP'd using MOG than in the nEVs, regardless of the neuronal marker used, validating their oligodendroglial origin [Figure 3C, Table 3]. Cytochrome C concentrations were in the low pg/mL concentration range for all the markers, though surprisingly, two of five biological replicates were ~2-times higher in the nEVs isolated using ATP1A3 compared to those isolated using the other three markers [Figure 3D, Table 3], possibly related to the role of this protein in neuronal autosis - an autophagy-related, non-canonical apoptosis pathway[48].

Table 3. Markers measured in EVs isolated using different surface antigens.

IP Marker	MAP-2[1]	GRIN2B	CNPase	Cytochrome C	Prominin-2	E-cadherin	GPA33	α-Synuclein	CKM

L1CAM	191 ± 34	592 ± 68	193 ± 18	23 ± 5	BDL[2]	BDL	251 ± 5	30.9 ± 0.9	BDL
GAP-43	202 ± 29	583 ± 128	158 ± 24	13 ± 4	BDL	BDL	64 ± 13	25 ± 3	BDL
NLGN3	234 ± 42	714 ± 155	160 ± 16	17 ± 3	BDL	BDL	27 ± 13	31 ± 1	BDL
ATP1A3	197 ± 27	521 ± 55	210 ± 39	42 ± 21	BDL	BDL	63 ± 27	17 ± 3	16 ± 5
MOG	33 ± 40	70 ± 39	2627 ± 487	21.0 ± 0.9	BDL	BDL	35 ± 12	ND[3]	BDL

[1]All the concentrations are in pg/mL. [2]BDL = below detection limit. [3]ND = Not determined.

According to the Protein Atlas (www.proteinatlas.org), in addition to the brain, L1CAM is present in several peripheral tissues, most prominently in renal distal tubules[49,50]. In the GI tract, L1CAM is expressed at low levels in glandular cells in the stomach and in endothelial cells in the colon[51]. In fact, it has been reported to be present on the membrane of EVs secreted by intestinal epithelial cells[52]. GAP-43 is also found at low levels in the GI tract, though only in peripheral nerves innervating the colon[53]. ATP1A3 is expressed in cardiomyocytes[54] in addition to the brain neurons. In contrast, NLGN3 has not been reported to be expressed in tissues or cells outside CNS neurons.

Prominin-2 and E-cadherin were present in the serum (2.8 ± 0.3 ng/mL and 2.5 ± 0.8 ng/mL, respectively) but were below the detection limit of the ELISA kits we used in total EVs precipitated from the serum using the ExoQuick kit (data not shown) or in EVs IP'd using any of the neuronal or oligodendroglial markers [Table 3]. These results were somewhat surprising as both proteins are membrane-associated and have been reported previously to be associated with EVs[55-58]. Thus, the absence of signal for either of these two markers in our experiments may reflect the specific antibody combinations in the ELISA kits we used.

Measurement of GPA33 showed concentrations near the detection limit of the assay in EVs IP'd using GAP-43, NLGN3, or ATP1A3, whereas an order of magnitude higher concentrations were detected in EVs isolated using L1CAM [Figure 1E, Table 3], demonstrating the lower neuronal specificity of this marker compared to the other three proteins. CKM was detected only in EVs IP'd using an anti-ATP1A3 antibody [Figure 3F,

Table 3], suggesting that a fraction of the EVs IP'd using ATP1A3 originated in cardiomyocytes.

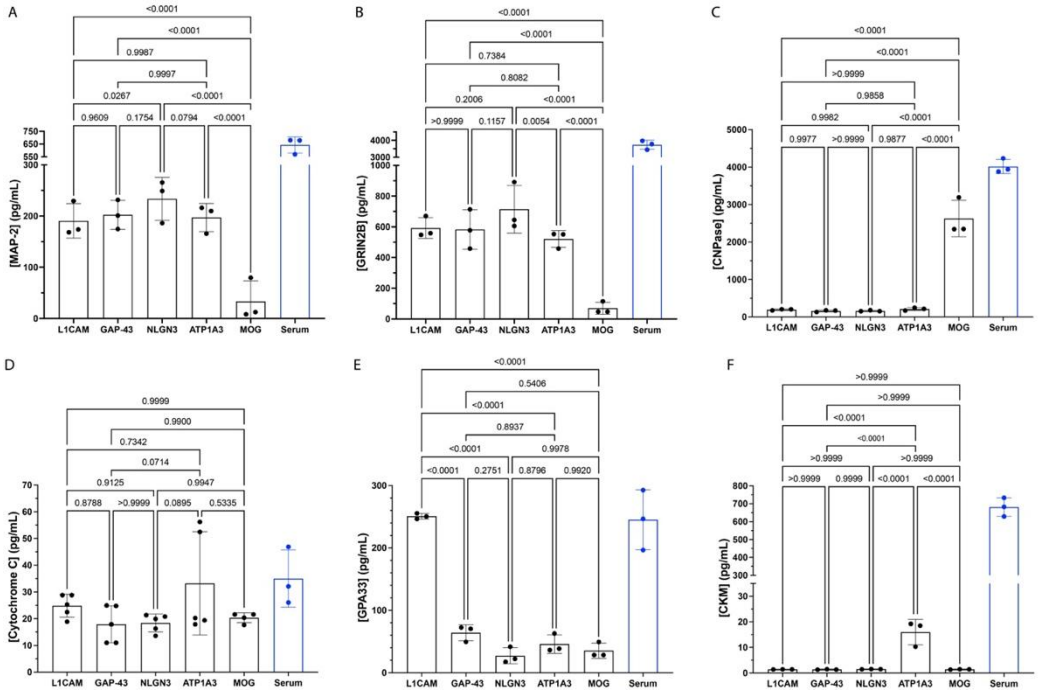

Figure 3. Analysis of cell-origin markers in EVs IP'd using neuronal or oligodendroglial surface proteins. EVs were IP'd using magnetic Dynabeads™ conjugated to monoclonal antibodies specific for L1CAM, GAP-43, NLGN3, ATP1A3, or MOG (Table 1). Cell-origin markers, including the neuronal markers A) MAP-2 and B) GRIN2B (data imputed for MOG); C) the oligodendroglial marker CNPase (data imputed for L1CAM, GAP-43, NLGN3, and ATP1A3); D) the apoptotic marker cytochrome C as a negative control; E) the GI marker GPA33; or F) the muscle marker CKM (Data imputed for L1CAM, GAP-43, NLGN3, and MOG) were quantified using commercial ELISA kits [Table 2]. An equal amount of total protein was loaded in each well. Unfractionated serum, not normalized by total protein content, was used as a positive control in each assay (blue columns) and was not included in the statistical analysis. Each data point represents an independent biological replicate performed in three technical replicates. P-values were calculated using a repeated-measure, two-way ANOVA with Tukey's correction for multiple comparisons.

Soluble L1CAM, but not GAP-43, NLGN3, or ATP1A3, co-precipitates with EVs.

As mentioned above, one of the reasons to doubt the utility of L1CAM as a marker for isolation of nEVs, despite its frequent use for this purpose[25], was its presence as a soluble protein in the blood and the demonstration that the concentration of the soluble forms was orders of magnitude higher than the concentration of membrane-tethered L1CAM on the surface of EVs[24,26]. To test whether a similar concern could be raised for the other markers we used for the IP of nEVs and oEVs, we used SDS-PAGE/western blots and tested for the presence of each marker in EVs isolated from serum using the ExoQuick kit compared to the remaining, EV-depleted serum. The preparations were normalized by loading 100 µg of total protein in each lane. Following SDS-PAGE and transfer to a nitrocellulose membrane, the membrane was probed using antibodies against each marker. In the L1CAM immunoblot, we observed in the EVs a high molecular weight form of L1CAM at ~210 kDa, which has been reported previously to be heavily glycosylated[59], along with two higher-mobility bands, likely representing immature post-translational modifications and/or proteolytic cleavage of the protein, as reported previously[60,61]. The analysis showed substantially more L1CAM in the EVs compared to the EV-depleted serum [Figure 4A, B], which may seem counterintuitive, but is simply a reflection of the normalization to total protein, which leads to a much higher concentration of L1CAM in the EVs. The protein content in the serum is ~13,500-times higher than in EVs[62]. When this ratio is considered in the calculation, it reveals that < 1% of L1CAM is EV-bound, whereas most of it exists in a soluble form in the serum or plasma, as reported earlier[27,63]. In contrast to L1CAM, no soluble GAP-43 [Figure 4C], NLGN3 [Figure 4D], or ATP1A3 [Figure 4E] were detected in the EV-free serum.

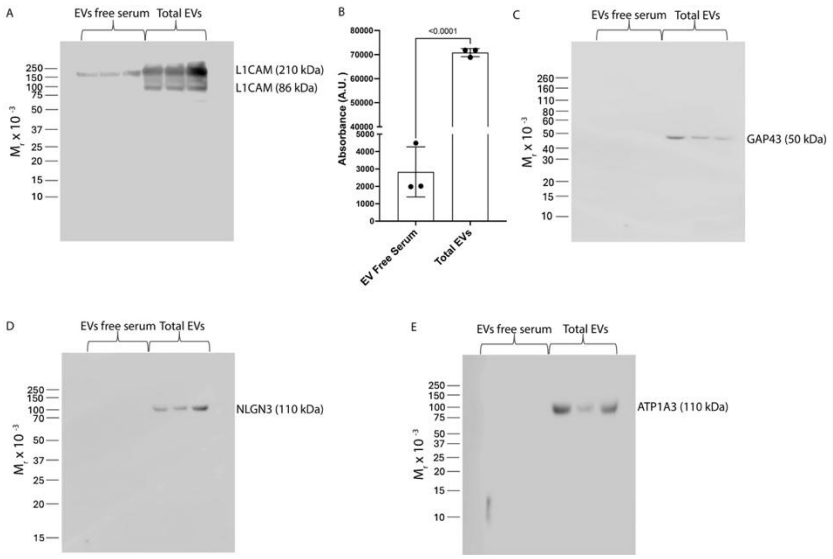

Figure 4. Western-blot analysis of proteins used as surface markers for IP of nEVs. nEVs were IP'd using antibodies against each neuronal marker. The captured EVs and the serum remaining after the capture were analyzed by western blots in three technical replicates each. 100 µg of total protein was loaded in each lane. A) A representative immunoblot probed for L1CAM; B) Densitometric quantification of three biological replicates of L1CAM immunoblots. The p-value was calculated using Welch's *t*-test; C) A representative immunoblot probed for GAP-43; D) A representative immunoblot probed for NLGN3; E) A representative immunoblot probed for ATP1A3.

NLGN3 is the preferred marker for measurement of α-syn in nEVs.

As NLGN3 yielded the highest concentration levels of the neuronal markers MAP-2 and GRIN2B [Figure 3A, B, Table 3], we hypothesized that it would also provide the highest signal of neuronal biomarkers measured in the nEVs. To test this hypothesis, we chose α-syn, a CNS protein that forms toxic oligomers and aggregates in Parkinson's disease and other neurodegenerative disorders[25,64,65], as a representative nEV biomarker. nEV α-syn was quantified using an ECLIA normalizing the measurements by loading an equal amount of total protein in each well.

The analysis showed that the nEV α-syn concentrations measured using L1CAM or NLGN3 were comparable to each other and significantly higher than those measured following IP using GAP-43 (19% lower than using L1CAM or NLGN3) or ATP1A3 (45% lower, Figure

5, Table 3). Because the specificity of L1CAM for CNS neurons is lower than that of NLGN3 [Figures 3A, B], we conclude that NLGN3 provides the highest combination of yield and specificity for measurement of α-syn, and possibly other neuronal biomarkers in nEVs.

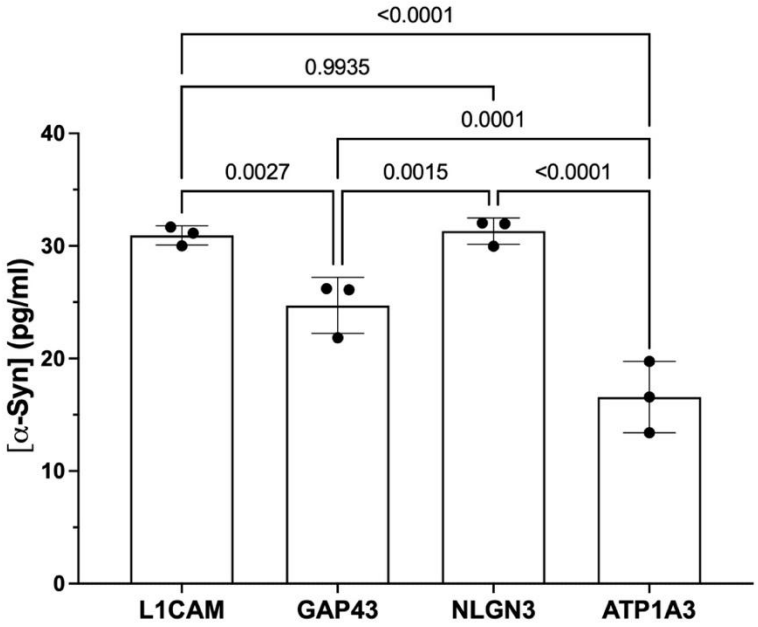

Figure 5. Measurement of α-syn in EVs IP'd using different neuronal surface markers. α-Syn was measured using an MSD ECLIA in EVs IP'd using magnetic Dynabeads™ conjugated to antibodies specific for L1CAM, GAP-43, NLGN3, or ATP1A3. 10 µg of total protein was loaded in each well. Each data point represents an independent biological replicate performed in three technical replicates. *P*-values were calculated using a repeated-measure, 2-way ANOVA with Tukey's correction for multiple comparisons.

Comparison of manual nEV isolation with an automated system.

As the IP step in our process involves the use of magnetic beads, to further streamline the process, we tested automating the steps following the IP step using a robotic platform. Several commercially available systems can be considered for this task, of which we compared a Stellar Scientific IsoPure system and a Thermo Fisher KingFisher Apex system. Both automated systems handle up to 96 samples using an array of magnetic pins that fit typical 96-well plates. The IsoPure system is substantially less expensive than the KingFisher Apex instrument, yet it is not equipped with a cooling system and has a larger dead volume

due to the broader magnetic tips this system uses. As our process requires eluting the EVs in a relatively small volume, 20-25 µL, the loss of sample in the IsoPure system was too large and ruled out further use of this system.

The KingFisher Apex includes a cooling system and accommodates narrow tips, allowing handling small eluate volumes, minimizing sample loss. The total protein measurement in the isolated EVs indicated a slight loss when isolating nEVs using the KingFisher Apex system (13.6 ± 0.5 µg) compared to manual isolation (15.6 ± 0.6 µg, Figure 6A). To assess the recovery of specific nEVs cargo, we measured α-syn concentration. Similar to the total protein measurement, the KingFisher Apex yielded a somewhat lower α-syn concentration, 35 ± 2 pg/mL, compared to the manual isolation (40 ± 5 pg/mL, Figure 6B). These results agreed with marginally lower average levels of syntenin-1 in the preparation isolated using the automated system [Figure 6C, D]. Notably, the coefficient of variation (CV) was lower using the automated system in all cases, suggesting improved precision. Together with the saving of experimenter's time and effort, these data support using the automated system, especially for high throughput applications, despite the small loss in yield.

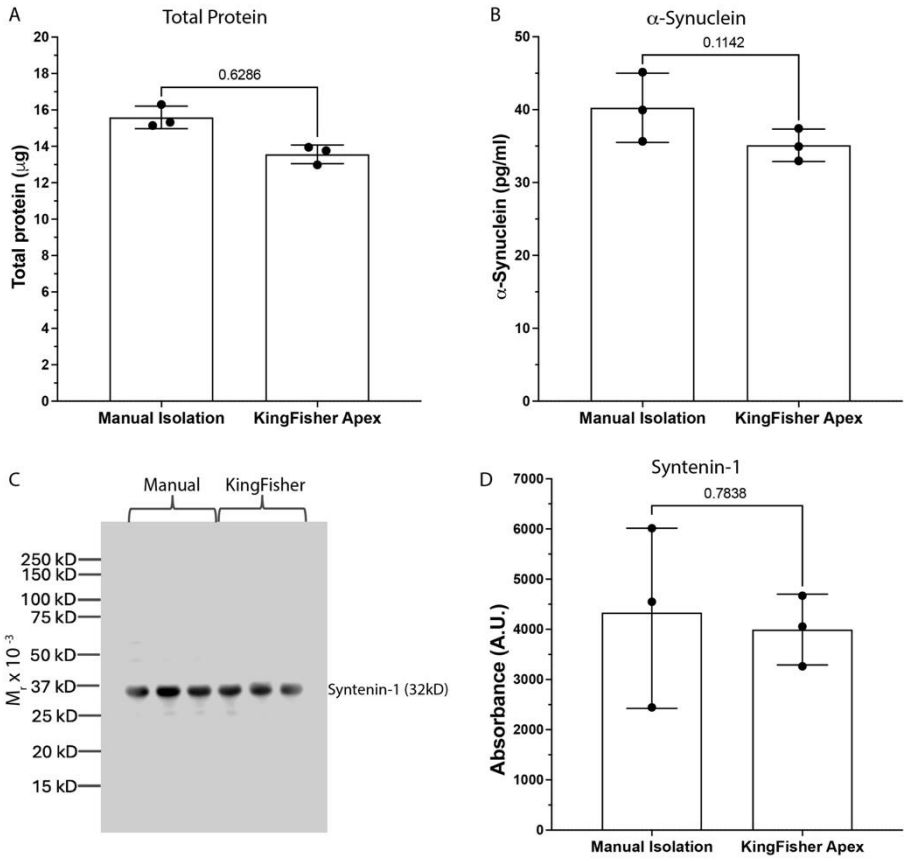

Figure 6. Comparison between manual EV isolation and a robotic system. nEVs were isolated from 200 µL of commercial human serum and then IP'd using an anti-NLGN3 antibody manually or by performing the wash and lysis steps using a KingFisher Apex system. A) Total protein yield; B) α-Syn measured in 10 µg of total nEVs protein; C) Syntenin-1 immunoblot; D) Densitometric analysis of syntenin-1 immunoblots. Each data point represents an independent biological replicate performed in three technical replicates. *P*-values were calculated using a repeated-measure, 2-way ANOVA with Tukey's correction for multiple comparisons.

Serial isolation of EVs originating in different cell types from a single sample aliquot. Our method for isolating cell-specific EVs, e.g., nEVs or oEVs, from blood products typically requires 200 µL of serum or plasma. Other groups have reported using 250 µL[66], 500 µL[67], or 1000 µL[68] of serum/plasma or CSF for similar purposes. The supernatant liquid remaining after the IP step theoretically contains all the non-targeted EVs except a small percentage that may bind non-specifically to the beads or antibodies. Thus, we reasoned

that isolation of EVs using a marker of a different cell type from the same sample should be feasible with a minimal loss in yield [Figure 1].

In a recent report, Camacho-Meño *et al.* used a similar for isolating EVs of neuronal, astroglial, oligodendroglial, and microglia/macrophage origin. They used 1,000 µL of starting serum volume and demonstrated that EVs originating in the different cell types could be isolated serially, yet they did not address the questions whether the yield of EVs from each cell type was impacted by the serial isolation or how the order of isolation might have affected the yield[35]. These questions become crucial when the available sample volume is limited. To address them, we compared the yield of nEVs and oEVs when IP'd using NLGN3 and MOG, respectively, successively from a single 200-µL aliquot and examined whether the order of isolation affected the yield. In view of the minimal yield loss and higher reproducibility using the KingFisher Apex system compared to manual isolation, we also evaluated whether the automated platform was compatible with sequential isolation. As readouts, following EV lysis we measured syntenin-1 by western blot, GRIN2B and CNPase by ELISA, and α-syn by ECLIA.

Immunoblotting for syntenin-1 was used to assess the total EVs isolated after each IP step in the manual [Figure 7A] or automated isolation [Figure 7B] methods. The densitometric absorbace of the bands was normalized to the highest value band in the three biological replicates (Figure 7C, orange dot). We found a 32 ± 4% decrease in yield when nEVs were isolated manually after oEVs, but only a 14 ± 4% decrease when oEVs were isolated after nEVs [Figure 7A, C]. Similarly, when the isolation was done using the KingFisher Apex, the yield decreased by 28 ± 4% when nEVs followed oEVs, and by 15 ± 2% when oEVs followed nEVs [Figure 7B, C].

Measurement of the neuronal marker GRIN2B in the nEVs yielded results consistent with the syntenin-1 analysis. Using manual isolation, GRIN2B levels dropped by 42%, from 444 ± 20 pg/mL when nEVs were IP'd first to 258 ± 35 pg/mL when nEVs were IP'd after isolation of oEVs. Similarly, following automated isolation using the KingFisher Apex, GRIN2B concentrations decreased by 47%, from 406 ± 20 pg/mL when nEVs were IP'd first

to 215 ± 24 pg/mL when nEVs were IP'd after isolation of oEVs [Figure 7D]. CNPase levels in the oEVs supported these results, decreasing by 21%, from 1,923 ± 248 pg/mL when oEVs were isolated first to 1,521 ± 120 pg/mL when oEVs were isolated manually after nEV isolation, and by 19%, from 1841 ± 51 to 1,490 ± 49 pg/mL, respectively, using the KingFisher Apex [Figure 7E]. Finally, assessing the impact of the serial isolation on α-syn as a representative CNS-originating EV biomarker [Figures 7F, G] demonstrated that isolation of nEVs after IP of oEVs decreased the α-syn concentration measured in the nEVs by 47%, from 50 ± 3 to 27 ± 4 pg/mL, whereas oEV α-syn concentrations decreased by 28%, from 40.6 ± 0.5 to 30 ± 1 pg/mL when oEVs were IP'd first or second using manual isolation, respectively [Figure 7F], and the trend was similar using the KingFisher Apex [Figure 7G]. Collectively, these data indicate that serial isolation of two (or more) EV sub-populations from a single sample is a viable strategy that may be important when sample volume is limited. The data indicate that the order of isolation affects the recovery of specific markers strongly and should be evaluated before deciding the sequence of isolation.

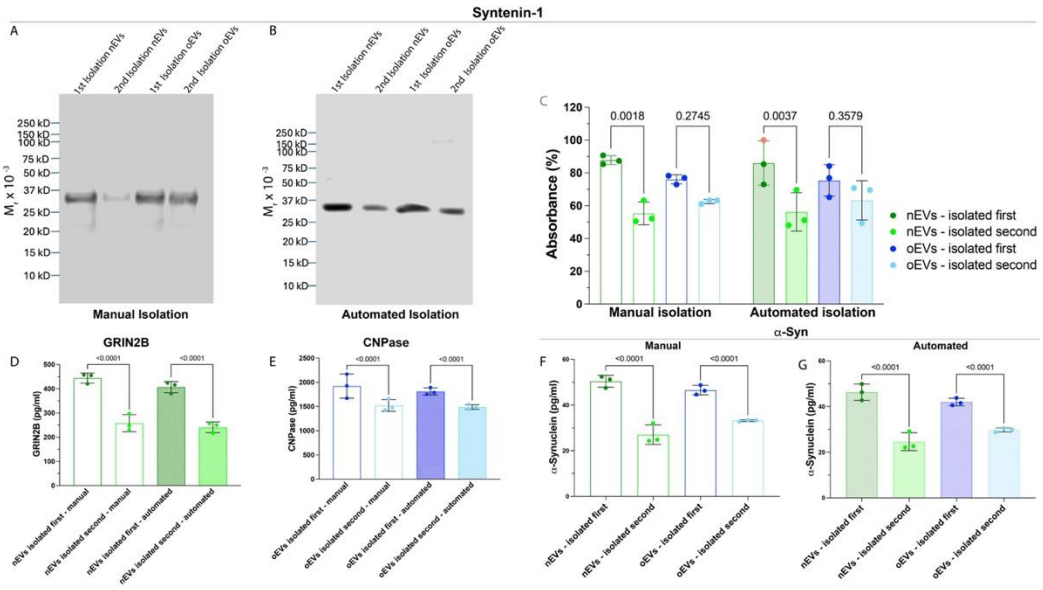

Figure 7. Comparison of isolation order in serial IP of nEVs and oEVs from the same sample. EVs were IP'd sequentially from the same aliquot, either manually or incorporating wash and lysis steps using the KinkFisher Apex system. Different markers were evaluated to assess the yield of the EVs in the first and second isolation. A, B) Representative immunoblots of syntenin-1 in nEVs and oEVs when isolated first or second, each A)

manually or B) using the KingFisher Apex system; C) Densitometric quantification of the immunoblots analysis. The orange dot represents the highest densitometric value to which all the other values were normalized; D) GRIN2B concentrations measured in nEVs when isolated first (before oEVs) or second (after oEVs), manually or using the KingFisher Apex; E) CNPase concentrations measured in oEVs when isolated first (before nEVs) or second (after nEVs) manually or using the KingFisher Apex; F, G) α-Syn concentration in nEVs and oEVs isolated serially in each order G) manually or F) using KingFisher Apex. Each data point represents an independent biological replicate performed in three technical replicates. *P*-values were calculated using a repeated-measure, 2-way ANOVA with Tukey's correction for multiple comparisons.

A duplex ECLIA for simultaneous measurement of total α-syn and p129-α-syn

As a group interested in synucleinopathies, two of the biomarkers we measure often are total α-syn and α-syn phosphorylated at Ser129 (pS129-α-syn). The latter is found at low levels in the normal brain[69], where it may be involved in synaptic remodeling[70], but is highly enriched in pathological deposits found in the brain and peripheral nerves of patients with synucleinopathies[69,71,72] and is used commonly as a marker of α-syn pathology. Recently, we developed a sensitive ECLIA for the measurement of pS129-α-syn that had a 14 ± 10 pg/mL sensitivity limit and > 10^5 selectivity for the phosphorylated form relative to unphosphorylated α-syn[73]. To further facilitate the measurement of both the total and phosphorylated forms of α-syn when sample volume is limited, here we aimed to develop a duplex assay capable of measuring both analytes simultaneously.

Because the assays use different antibodies for capture but the same antibody for detection, we could use semi-synthetic pS129-α-syn[74] as the standard for both the total α-syn and pS129-α-syn measurements. To create multiplex, home-brewed assays, MSD provides 96-well plates with 10 spots printed per well and a set of unique linkers allowing attachment of up to 10 different capture antibodies. We selected to use spots/linkers 1 and 10 for attaching the biotinylated capture antibodies. Linker 1 was attached to antibody EP1536Y, specific for pS129-α-syn antibody[75], whereas linker 10 was attached to the biotinylated anti-total-α-syn antibody provided by MSD in the U-PLEX Human α-Synuclein kit.

Initial experiments showed that the signal of total α-syn was > 20-times higher than that of pS129-α-syn. Possible explanations are that the total α-syn capture antibody provided by MSD has a substantially higher affinity for the protein than that of antibody EP1536Y for pS129-α-syn, the undisclosed concentration of the MSD capture antibody is higher than the one we used for EP1536Y, or the attachment of the total α-syn capture antibody was substantially more efficient than that of EP1536Y. Switching the position of the antibodies did not change the difference in the signal (data not shown). To address this large signal difference, we diluted the total α-syn capture antibody serially while keeping the concentration of EP1536Y constant at 2 µg/mL. Diluting the total α-syn capture antibody 1:10 yielded similar signals for both total α-syn and pS129-α-syn, allowing meaningful comparison of the duplex assay to the individual single-capture-antibody assays under these conditions.

As pS129-α-syn levels are often below detection levels in healthy human serum or wild-type mouse brain extracts, we used a brain extract from an MSA transgenic mouse[38], which contains a high concentration of pS129-α-syn[76], and nEVs isolated from the serum of a patient with MSA used in a previous study[26] to compare the singlex and duplex assays. Equal aliquots of the sample were used in both assay formats. We found comparable concentrations of both ps129-α-syn and total α-syn concentrations using the singlex (ps129-α-syn 8,651 ± 1,388 pg/mL, total α-syn 113,920 ± 11,420 pg/mL) compared to the duplex assay (ps129-α-syn 10,123 ± 1,296 pg/mL, total α-syn 101,854 ± 10,844 pg/mL, Figure 8A). Similarly, equal amounts of total protein in nEVs from an MSA serum sample yielded comparable concentrations of pS129-α-syn and total α-syn, 19 ± 5 pg/mL pS129-α-syn in the singlex assay compared to 17 ± 3 pg/mL in the duplex assay, and 248 ± 62 pg/mL compared to 264 ± 34 pg/mL total α-syn, respectively [Figure 8B].

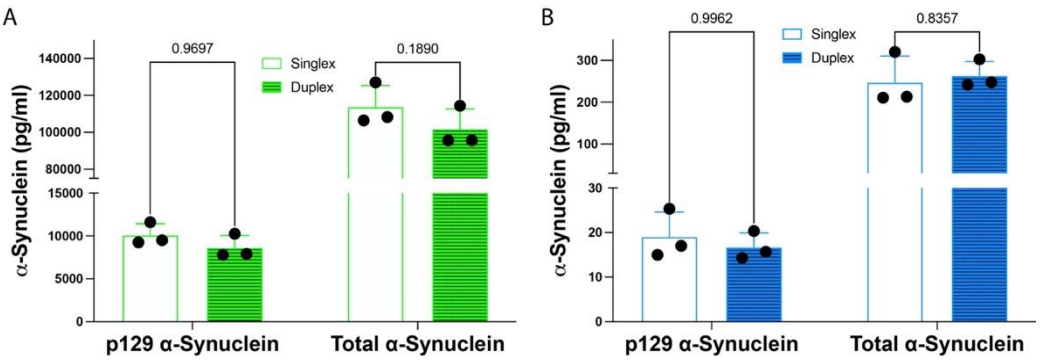

Figure 8. Comparison of singlex and duplex assays for the measurements of total α-syn and pS129-α-syn. A) Total α-syn and pS129-α-syn were measured in an MSA mouse brain extract. 15 µg of total protein was loaded in each well; B) Total α-syn and pS129-α-syn were measured in nEVs isolated from the serum of a patient with MSA. 10 µg of total protein was loaded in each well. Each data point represents an independent biological replicate performed in three technical replicates. *P*-values were calculated using a repeated-measure, 2-way ANOVA with Tukey's correction for multiple comparisons.

DISCUSSION

Several dozen papers, including from our group[26,77,78], have reported using immunocapture of nEVs using anti-L1CAM antibodies (51 papers reviewed in 2022[79] and more published since then). Despite the popularity of this marker, its expression in peripheral tissues and high concentration of soluble forms in the blood compared to the surface of EVs has sparked significant debate[24,25], leading to exploration of other potential markers for IP of nEVs from biological fluids. Our comparison of L1CAM with recently reported alternatives, including GAP-43[28], NLGN3[28], and ATP1A3[29] suggests that NLGN3 is superior to the other markers in terms of nEV yield [Figure 3A, B] and specificity [Figure 3E, F]. The difference in yield is relatively small, roughly 20%, and based on measurements of the neuronal markers MAP-2 [Figure 3A] and GRIN2B [Figure 3B] was not statistically meaningful in all cases, yet these measruements agree also with the higher concentration of α-syn found in the nEVs isolated using NLGN3 [Figure 5] and support the conclusion that isolation of nEVs using NLGN3 yields the highest signal of candidate CNS neuronal biomarkers among the four markers examined. The concentration of α-syn measured in L1CAM-isolated nEVs was similar to that in nEVs isolated using NLGN3, yet the higher likelihood that a fraction of EV-

attached L1CAM originated in peripheral tissues [Figures 3E, 4A] further supports NLGN3 as the marker of choice for nEV isolation. Our study also confirms the high specificity of MOG for isolation of oEVs [Figure 3, Table 3].

Additionally, addressing the labor-intensive nature of cell-specific EV isolation, we demonstrate that replacing manual wash and lysis steps in the isolation process of cell-specific EVs following IP with a robotic device can lead to substantial saving in human effort and increase precision, with a minimal loss of yield [Figure 6].

Another practical issue limiting EV biomarker discovery is the low sample volume often available in various biorepository. To date, immunocapture of EVs from biological samples has been done in most studies by dedicating an aliquot to a single EV type, most commonly nEVs, whereas the remainder of the sample typically was discarded after this step. We demonstrate here that isolation of EVs originating in two distinct cell types, neurons and oligodendrocytes, is feasible, albeit with a 15-20% loss in yield for the second isolation and can be adapted to using the KingFisher Apex system [Figure 7]. In view of the scarcity of patient samples and the advantage of testing biomarkers in EVs from multiple cellular origins, sequential isolation may be advantageous for future EV biomarker studies.

Importantly, in the sequential isolation experiments, we found that the order of EV isolation affected the yield substantially. When nEVs were isolated after oEVs, the signal loss was more than doubled compared to alternative order [Figure 7]. A possible explanation is non-specific binding of EVs to the beads, antibodies, or surface of the vial. Our data suggest that nEVs may bind nonspecifically to these entities to a larger extent than oEVs.

Another strategy for enhancing sample utilization is multiplexing, allowing measurement of more than one analyte in each sample. To this end, we developed a duplex assay that simultaneously measures α-syn and pS129-α-syn in the same sample using a high-sensitivity ECLIA. Assay optimization required testing various dilutions of the α-syn antibody to obtain comparable raw signals for the two analytes. A 1:10 dilution was found to be optimal,

allowing detection of both α-syn and pS129-α-syn at comparable levels to those of the single-antibody assays in both human and mouse samples [Figure 8].

Limitations of our study include using exclusively serum and no other biofluids for the comparison among the markers, and not including other, recently published potential markers for nEV isolation, such as glutamate ionotropic receptor NMDA-type subunit 2A[80].

Conclusion

This study critically assesses nEV isolation markers and addresses the debate over L1CAM's specificity. Our comparison finds NLGN3 to be a preferable marker compared to L1CAM, ATP1A3, or GAP-43, providing a somewhat higher yield and better specificity for neuronal EVs originating in the CNS. Additionally, we show that sequential immunoaffinity purification is an effective approach for analyzing EV from multiple cell types. By first isolating nEVs and then oEVs from the same sample, researchers can maintain high yields of both EV types, overcoming the challenge of limited clinical biospecimen availability. Finally, our home-brewed duplex ECLIA measures α-syn and pS129-α-syn in a single sample with comparable sensitivity to the respective singlex assays.

DECLARATIONS

Acknowledgment

The EV characterization work, including NTA and ExoView, was performed at the Extracellular Vesicle and Nanoparticle Analytics (EV-NP) at The Saban Research Institute, Children's Hospital Los Angeles. We thank Drs. Paolo Neviani, and Khairat El-Baradie for their help with these experiments.

Authors' contributions

Conceptualization, Methodology, Investigation, Validation, Formal analysis, Writing-original draft: Siddique I;

Methodology, Data curation, Formal analysis: Wang Y, Khijniak M, Hong M;

Contribution of crucial materials, Critical reading of the manuscript: Stefanova N;

Conceptualization, Methodology, Supervision, Writing, Editing: Bitan G;

All authors have read and agreed to the published version of the manuscript.

Availability of data and materials

The dataset supporting the conclusions of this article are deposited in Open Science Framework.

AI and AI-assisted tools statement

During the preparation of this manuscript, the authors used Gemini (Google) to assist in the creation of certain parts of the Graphical Abstract. After using this tool, the authors reviewed and edited the content as needed and took full responsibility for the accuracy and integrity of the final illustration. AI tools were not used for data collection, data analysis, or writing the manuscript.

Financial support and sponsorship

The project was supported by NIH/NINDS grants RF1NS126406, R21NS130326, and R21NS137072 (GB). MH was supported by a Whitcome Fellowship and by Supplement RF1NS126406-01A1S1.

Conflicts of interest

GB is an Associate Editor of "Extracellular Vesicles and Circulating Nucleic Acids" and was not involved in any steps of editorial processing, notably including reviewer selection, manuscript handling, and decision making. The other authors declare no conflicts of interest. IS and GB are co-authors and co-inventors of International Patent Application No. PCT/US24/13520, US application No. 19/146,842, EU application No. 24750856.7. The other authors declare no conflicts of interest.

Ethical approval and consent to participate

Pooled human serum was obtained from Innovative Research (Novi, MI). It was ethically sourced by the vendor in accordance with approved protocols and donor consent. Blood-collection from the patient with MSA whose sample was used for the analysis shown in Figure 8 was approved by the Human Subjects Committees of UCLA and NYU for a previous

study[26]. The researchers performing the analysis did not have access to any identifiable information. The mouse brain sample used for the analysis shown in Figure 8 was obtained for a previous study[76] in accordance with the Austrian law under permission BMWFW-66.011/0018-WF/V/3b/2015.

Consent for publication

Not Applicable.

Copyright

REFERENCES

1. Mathieu M, Martin-Jaular L, Lavieu G, Thery C. Specificities of secretion and uptake of exosomes and other extracellular vesicles for cell-to-cell communication. *Nat Cell Biol* 2019;21:9-17.[PMID: 30602770 DOI: 10.1038/s41556-018-0250-9]

2. van Niel G, D'Angelo G, Raposo G. Shedding light on the cell biology of extracellular vesicles. *Nat Rev Mol Cell Biol* 2018;19:213-28.[PMID: 29339798 DOI: 10.1038/nrm.2017.125]

3. Anand S, Samuel M, Kumar S, Mathivanan S. Ticket to a bubble ride: Cargo sorting into exosomes and extracellular vesicles. *Biochim Biophys Acta Proteins Proteom* 2019;1867:140203.[PMID: 30822540 DOI: 10.1016/j.bbapap.2019.02.005]

4. Buzas EI. The roles of extracellular vesicles in the immune system. *Nat Rev Immunol* 2023;23:236-50.[PMID: 35927511 PMCID: PMC9361922 DOI: 10.1038/s41577-022-00763-8]

5. Pitt JM, Kroemer G, Zitvogel L. Extracellular vesicles: masters of intercellular communication and potential clinical interventions. *J Clin Invest* 2016;126:1139-43.[PMID: 27035805 PMCID: PMC4811136 DOI: 10.1172/JCI87316]

6. Takeuchi T. Pathogenic and protective roles of extracellular vesicles in neurodegenerative diseases. *J Biochem* 2021;169:181-6.[PMID: 33196835 DOI: 10.1093/jb/mvaa131]

7. Kisielewska M, Rakoczy K, Skowron I, et al. Utilizing Extracellular Vesicles for Eliminating 'Unwanted Molecules': Harnessing Nature's Structures in Modern Therapeutic

Strategies. *Molecules* 2024;29.[PMID: 38474460 PMCID: PMC10935043 DOI: 10.3390/molecules29050948]

8. Thery C, Amigorena S, Raposo G, Clayton A. Isolation and characterization of exosomes from cell culture supernatants and biological fluids. *Curr Protoc Cell Biol* 2006;Chapter 3:Unit 3 22.[PMID: 18228490 DOI: 10.1002/0471143030.cb0322s30]

9. Yates AG, Pink RC, Erdbrugger U, et al. In sickness and in health: The functional role of extracellular vesicles in physiology and pathology in vivo: Part I: Health and Normal Physiology: Part I: Health and Normal Physiology. *J Extracell Vesicles* 2022;11:e12151.[PMID: 35041249 PMCID: PMC8765331 DOI: 10.1002/jev2.12151]

10. Hornung S, Dutta S, Bitan G. CNS-Derived Blood Exosomes as a Promising Source of Biomarkers: Opportunities and Challenges. *Front Mol Neurosci* 2020;13:38.[PMID: 32265650 PMCID: PMC7096580 DOI: 10.3389/fnmol.2020.00038]

11. Fiandaca MS, Kapogiannis D, Mapstone M, et al. Identification of preclinical Alzheimer's disease by a profile of pathogenic proteins in neurally derived blood exosomes: A case-control study. *Alzheimers Dement* 2015;11:600-7 e1.[PMID: 25130657 PMCID: PMC4329112 DOI: 10.1016/j.jalz.2014.06.008]

12. Da Conceicao ARR, Marinatto J, Pinheiro LS, Rody T, De Felice FG. The Multifaceted Role of Extracellular Vesicles in Alzheimer's Disease. *J Neurochem* 2025;169:e70209.[PMID: 40862476 PMCID: PMC12382324 DOI: 10.1111/jnc.70209]

13. Kapogiannis D, Mustapic M, Shardell MD, et al. Association of Extracellular Vesicle Biomarkers With Alzheimer Disease in the Baltimore Longitudinal Study of Aging. *JAMA Neurol* 2019;76:1340-51.[PMID: 31305918 PMCID: PMC6632160 DOI: 10.1001/jamaneurol.2019.2462]

14. Shi M, Liu C, Cook TJ, Bullock KM, Zhao Y, et al. Plasma exosomal α-synuclein is likely CNS-derived and increased in Parkinson's disease. *Acta Neuropathol* 2014;128:639-50.[PMID: 24997849 PMCID: PMC4201967 DOI: 10.1007/s00401-014-1314-y]

15. Xylaki M, Chopra A, Weber S, et al. Extracellular Vesicles for the Diagnosis of Parkinson's Disease: Systematic Review and Meta-Analysis. *Mov Disord* 2023;38:1585-97.[PMID: 37449706 DOI: 10.1002/mds.29497]

16. Zhang S, Li J, Hu X, et al. Brain-derived extracellular vesicles: A promising avenue for Parkinson's disease pathogenesis, diagnosis, and treatment. *Neural Regen Res* 2026;21:1447-67.[PMID: 40313118 PMCID: PMC12407533 DOI: 10.4103/NRR.NRR-D-24-01262]

17. Khadka A, Spiers JG, Cheng L, Hill AF. Extracellular vesicles with diagnostic and therapeutic potential for prion diseases. *Cell Tissue Res* 2023;392:247-67.[PMID: 35394216 PMCID: PMC10113352 DOI: 10.1007/s00441-022-03621-0]

18. Darabi S, Ariaei A, Rustamzadeh A, et al. Cerebrospinal fluid and blood exosomes as biomarkers for amyotrophic lateral sclerosis; a systematic review. *Diagn Pathol* 2024;19:47.[PMID: 38429818 PMCID: PMC10908104 DOI: 10.1186/s13000-024-01473-6]

19. McCluskey G, Morrison KE, Donaghy C, et al. Extracellular Vesicles in Amyotrophic Lateral Sclerosis. *Life (Basel)* 2022;13.[PMID: 36676070 PMCID: PMC9867379 DOI: 10.3390/life13010121

20. Ghosh M, Bayat AH, Pearse DD. Small Extracellular Vesicles in Neurodegenerative Disease: Emerging Roles in Pathogenesis, Biomarker Discovery, and Therapy. *Int J Mol Sci* 2025;26.[PMID: 40806377 PMCID: PMC12346766 DOI: 10.3390/ijms26157246]

21. Thompson AG, Gray E, Heman-Ackah SM, et al. Extracellular vesicles in neurodegenerative disease - pathogenesis to biomarkers. *Nat Rev Neurol* 2016;12:346-57.[PMID: 27174238 DOI: 10.1038/nrneurol.2016.68]

22. Samatov TR, Wicklein D, Tonevitsky AG. L1CAM: Cell adhesion and more. *Prog Histochem Cytochem* 2016;51:25-32.[PMID: 27267927 DOI: 10.1016/j.proghi.2016.05.001]

23. Angiolini F, Belloni E, Giordano M, et al. A novel L1CAM isoform with angiogenic activity generated by NOVA2-mediated alternative splicing. *Elife* 2019;8.[PMID: 30829570 PMCID: PMC6398979 DOI: 10.7554/eLife.44305]

24. Norman M, Ter-Ovanesyan D, Trieu W, et al. L1CAM is not associated with extracellular vesicles in human cerebrospinal fluid or plasma. *Nat Methods* 2021;18:631-4.[PMID: 34092791 PMCID: PMC9075416 DOI: 10.1038/s41592-021-01174-8]

25. Dutta S, Hornung S, Taha HB, Bitan G. Biomarkers for parkinsonian disorders in CNS-originating EVs: promise and challenges. *Acta Neuropathol* 2023;145:515-40.[PMID: 37012443 PMCID: PMC10071251 DOI: 10.1007/s00401-023-02557-1]

26. Dutta S, Hornung S, Kruayatidee A, et al. α-Synuclein in blood exosomes immunoprecipitated using neuronal and oligodendroglial markers distinguishes Parkinson's

disease from multiple system atrophy. *Acta Neuropathol* 2021;142:495-511.[PMID: 33991233 PMCID: PMC8357708 DOI: 10.1007/s00401-021-02324-0]

27. Nogueras-Ortiz CJ, Eren E, Yao P, et al. Single-extracellular vesicle (EV) analyses validate the use of L1 Cell Adhesion Molecule (L1CAM) as a reliable biomarker of neuron-derived EVs. *J Extracell Vesicles* 2024;13:e12459.[PMID: 38868956 PMCID: PMC11170079 DOI: 10.1002/jev2.12459]

28. Eitan E, Thornton-Wells T, Elgart K, et al. Synaptic proteins in neuron-derived extracellular vesicles as biomarkers for Alzheimer's disease: novel methodology and clinical proof of concept. *Extracell Vesicles Circ Nucl Acids* 2023;4:133-50.[PMID: 37842184 PMCID: PMC10568955 DOI: 10.20517/evcna.2023.13]

29. You Y, Zhang Z, Sultana N, et al. ATP1A3 as a target for isolating neuron-specific extracellular vesicles from human brain and biofluids. *Sci Adv* 2023;9:eadi3647.[PMID: 37713494 PMCID: PMC10881047 DOI: 10.1126/sciadv.adi3647]

30. Delgado-Peraza F, Nogueras-Ortiz CJ, Volpert O, et al. Neuronal and Astrocytic Extracellular Vesicle Biomarkers in Blood Reflect Brain Pathology in Mouse Models of Alzheimer's Disease. *Cells* 2021;10.[PMID: 33922642 PMCID: PMC8146429 DOI: 10.3390/cells10050993]

31. Goetzl EJ, Schwartz JB, Abner EL, Jicha GA, Kapogiannis D. High complement levels in astrocyte-derived exosomes of Alzheimer disease. *Annals of Neurology* 2018;83:544-52.[PMID: 29406582 PMCID: PMC5867263 DOI: 10.1002/ana.25172]

32. Winston CN, Goetzl EJ, Schwartz JB, Elahi FM, Rissman RA. Complement protein levels in plasma astrocyte-derived exosomes are abnormal in conversion from mild cognitive impairment to Alzheimer's disease dementia. *Alzheimers Dement (Amst)* 2019;11:61-6.[PMID: 31032394 PMCID: PMC6477776 DOI: 10.1016/j.dadm.2018.11.002]

33. Yu Z, Shi M, Stewart T, Fernagut PO, et al. Reduced oligodendrocyte exosome secretion in multiple system atrophy involves SNARE dysfunction. *Brain* 2020;143:1780-97.[PMID: 32428221 PMCID: PMC7296853 DOI: 10.1093/brain/awaa110]

34. Kim HK, Ju H, Chung YH, et al. Serum sEV miRNAs as Biomarkers in Myelin Oligodendrocyte Glycoprotein Antibody-Associated Disease. *Mol Neurobiol* 2025;62:12280-95.[PMID: 40388105 PMCID: PMC12367994 DOI: 10.1007/s12035-025-04932-3]

35. Camacho-Meno L, Labandeira CM, Bravo SB, et al. Brain-derived extracellular vesicle proteomics reveals neuroprotection induced by the ARB candesartan in Parkinson's disease patients. *NPJ Parkinsons Dis* 2025;12:19.[PMID: 41366251 PMCID: PMC12804683 DOI: 10.1038/s41531-025-01230-6]

36. Siddique I, Hong, M., Mohseni, K., Bidoki, S., Bitan, G. . Isolation of CNS-Originating Extracellular Vesicles from Blood and Cell Culture Media. In: editor^editors, editor. Extracellular Vesicles. Neuromethods. Humana, New York, NY:SPRINGER NATURE;2026.[DOI: 10.1007/978-1-0716-4905-3_4]

37. Yang H, Leland JK, Yost D, Massey RJ. Electrochemiluminescence: a new diagnostic and research tool. ECL detection technology promises scientists new "yardsticks" for quantification. *Biotechnology (N Y)* 1994;12:193-4.[PMID: 7764436 DOI: 10.1038/nbt0294-193]

38. Kahle PJ, Neumann M, Ozmen L, et al. Hyperphosphorylation and insolubility of α-synuclein in transgenic mouse oligodendrocytes. *EMBO Rep* 2002;3:583-8.[PMID: 12034752 PMCID: PMC1084143 DOI: 10.1093/embo-reports/kvf109]

39. Johns TG, Bernard CC. The structure and function of myelin oligodendrocyte glycoprotein. *J Neurochem* 1999;72:1-9.[PMID: 9886048 DOI: 10.1046/j.1471-4159.1999.0720001.x]

40. Rajesh S, Bago R, Odintsova E, et al. Binding to syntenin-1 protein defines a new mode of ubiquitin-based interactions regulated by phosphorylation. *J Biol Chem* 2011;286:39606-14.[PMID: 21949238 PMCID: PMC3234783 DOI: 10.1074/jbc.M111.262402]

41. DeGiosio RA, Grubisha MJ, MacDonald ML, et al. More than a marker: potential pathogenic functions of MAP2. *Front Mol Neurosci* 2022;15:974890.[PMID: 36187353 PMCID: PMC9525131 DOI: 10.3389/fnmol.2022.974890]

42. Sabo SL, Lahr JM, Offer M, Weekes A, Sceniak MP. GRIN2B-related neurodevelopmental disorder: current understanding of pathophysiological mechanisms. *Front Synaptic Neurosci* 2022;14:1090865.[PMID: 36704660 PMCID: PMC9873235 DOI: 10.3389/fnsyn.2022.1090865]

43. Lee J, Gravel M, Zhang R, Thibault P, Braun PE. Process outgrowth in oligodendrocytes is mediated by CNP, a novel microtubule assembly myelin protein. *J Cell Biol* 2005;170:661-73.[PMID: 16103231 PMCID: PMC2171497 DOI: 10.1083/jcb.200411047]

44. Zorova LD, Kovalchuk SI, Popkov VA, et al. Do Extracellular Vesicles Derived from Mesenchymal Stem Cells Contain Functional Mitochondria? *Int J Mol Sci* 2022;23.[PMID: 35806411 PMCID: PMC9266972 DOI: 10.3390/ijms23137408]

45. Xiao D, Ohlendorf J, Chen Y, et al. Identifying mRNA, microRNA and protein profiles of melanoma exosomes. *PLoS One* 2012;7:e46874.[PMID: 23056502 PMCID: PMC3467276 DOI: 10.1371/journal.pone.0046874]

46. Jaffer F, Avbersek A, Vavassori R, et al. Faulty cardiac repolarization reserve in alternating hemiplegia of childhood broadens the phenotype. *Brain* 2015;138:2859-74.[PMID: 26297560 PMCID: PMC4671482 DOI: 10.1093/brain/awv243]

47. Bidzimou MK, Muralidharan P, Zhang Z, et al. D801N in ATP1A3-encoded Na/K-ATPase α 3 causes cardiac arrhythmogenesis through sodium-calcium exchanger-mediated calcium overload. *JCI Insight* 2026;11.[PMID: 41948929 PMCID: PMC13134723 DOI: 10.1172/jci.insight.197721]

48. Depierre P, Ginet V, Truttmann AC, Puyal J. Neuronal autosis is Na(+)/K(+)-ATPase alpha 3-dependent and involved in hypoxic-ischemic neuronal death. *Cell Death Dis* 2024;15:363.[PMID: 38796484 PMCID: PMC11127954 DOI: 10.1038/s41419-024-06750-2]

49. Allory Y, Audard V, Fontanges P, Ronco P, Debiec H. The L1 cell adhesion molecule is a potential biomarker of human distal nephron injury in acute tubular necrosis. *Kidney Int* 2008;73:751-8.[PMID: 18059459 DOI: 10.1038/sj.ki.5002640]

50. Debiec H, Christensen EI, Ronco PM. The cell adhesion molecule L1 is developmentally regulated in the renal epithelium and is involved in kidney branching morphogenesis. *J Cell Biol* 1998;143:2067-79.[PMID: 9864376 PMCID: PMC2175226 DOI: 10.1083/jcb.143.7.2067]

51. Flaviana C, Monica P, Terenzio C, et al. L1CAM expression in human gastrointestinal tract development: From tongue to colon-rectum. *J Public Health Res* 2023;12:22799036231165624.[PMID: 37213825 PMCID: PMC10192797 DOI: 10.1177/22799036231165624]

52. van Niel G, Raposo G, Candalh C, et al. Intestinal epithelial cells secrete exosome-like vesicles. *Gastroenterology* 2001;121:337-49.[PMID: 11487543 DOI: 10.1053/gast.2001.26263]

53. Vento P, Soinila S. Quantitative comparison of growth-associated protein GAP-43, neuron-specific enolase, and protein gene product 9.5 as neuronal markers in mature human intestine. *J Histochem Cytochem* 1999;47:1405-16.[PMID: 10544214 DOI: 10.1177/002215549904701107]

54. Hauck C, Potter T, Bartz M, et al. Isoform specificity of cardiac glycosides binding to human Na+,K+-ATPase alpha1beta1, alpha2beta1 and alpha3beta1. *Eur J Pharmacol* 2009;622:7-14.[PMID: 19751721 PMCID: PMC4948948 DOI: 10.1016/j.ejphar.2009.08.039]

55. Bänfer S, Kutscher S, Fleck F, et al. Late domain dependent E-cadherin recruitment into extracellular vesicles. *Front Cell Dev Biol* 2022;10:878620.[PMID: 36172289 PMCID: PMC9511404 DOI: 10.3389/fcell.2022.878620]

56. Brown CW, Amante JJ, Chhoy P, et al. Prominin2 Drives Ferroptosis Resistance by Stimulating Iron Export. *Dev Cell* 2019;51:575-86.e4.[PMID: 31735663 PMCID: PMC8316835 DOI: 10.1016/j.devcel.2019.10.007]

57. Paris J, Wilhelm C, Lebbé C, et al. PROM2 overexpression induces metastatic potential through epithelial-to-mesenchymal transition and ferroptosis resistance in human cancers. *Clinical and Translational Medicine* 2024;14:e1632.[PMID: 38515278 PMCID: PMC10958126 DOI: 10.1002/ctm2.1632]

58. Wang B, Tan Z, Guan F. Tumor-Derived Exosomes Mediate the Instability of Cadherins and Promote Tumor Progression. *Int J Mol Sci* 2019;20.[PMID: 31357383 PMCID: PMC6696460 DOI: 10.3390/ijms20153652]

59. Fogel M, Gutwein P, Mechtersheimer S, et al. L1 expression as a predictor of progression and survival in patients with uterine and ovarian carcinomas. *Lancet* 2003;362:869-75.[PMID: 13678974 DOI: 10.1016/S0140-6736(03)14342-5]

60. Nayeem N, Silletti S, Yang X, et al. A potential role for the plasmin(ogen) system in the posttranslational cleavage of the neural cell adhesion molecule L1. *J Cell Sci* 1999;112 (Pt 24):4739-49.[PMID: 10574721 DOI: 10.1242/jcs.112.24.4739]

61. Faissner A, Teplow DB, Kubler D, et al. Biosynthesis and membrane topography of the neural cell adhesion molecule L1. *EMBO J* 1985;4:3105-13.[PMID: 4092678 PMCID: PMC554629 DOI: 10.1002/j.1460-2075.1985.tb04052.x]

62. Muraoka S, Hirano M, Isoyama J, et al. Comprehensive proteomic profiling of plasma and serum phosphatidylserine-positive extracellular vesicles reveals tissue-specific proteins. *iScience* 2022;25:104012.[PMID: 35340435 PMCID: PMC8941215 DOI: 10.1016/j.isci.2022.104012]

63. Ter-Ovanesyan D, Norman M, Lazarovits R, et al. Framework for rapid comparison of extracellular vesicle isolation methods. *Elife* 2021;10.[PMID: 34783650 PMCID: PMC8651285 DOI: 10.7554/eLife.70725]

64. Gilboa T, Ter-Ovanesyan D, Wang SC, et al. Measurement of alpha-synuclein as protein cargo in plasma extracellular vesicles. *Proc Natl Acad Sci U S A* 2024;121:e2408949121.[PMID: 39475636 PMCID: PMC11551346 DOI: 10.1073/pnas.2408949121]

65. Goedert M, Jakes R, Spillantini MG. The Synucleinopathies: Twenty Years On. *J Parkinsons Dis* 2017;7:S51-69.[PMID: 28282814 PMCID: PMC5345650 DOI: 10.3233/JPD-179005]

66. Goetzl EJ, Wolkowitz OM, Srihari VH, et al. Abnormal levels of mitochondrial proteins in plasma neuronal extracellular vesicles in major depressive disorder. *Mol Psychiatry* 2021;26:7355-62.[PMID: 34471251 PMCID: PMC8872999 DOI: 10.1038/s41380-021-01268-x]

67. Manolopoulos A, Mustapic M, Nogueras-Ortiz C, et al. Cognitive Resilience in Apolipoprotein epsilon4 Carrier Women Predicted by Neuron-Derived Extracellular Vesicles. *Ann Clin Transl Neurol* 2025;12:2097-106.[PMID: 40665589 PMCID: PMC12516249 DOI: 10.1002/acn3.70143]

68. Dmitry Ter-Ovanesyan (1)# SW, Tal Gilboa (1), Emma JK Kowal (1, 2), Wendy, Trieu (1) SI, 3), Bogdan Budnik (1), Clarissa May Babila (1), Graham Heimberg, (4) MWB, Hasmik Keshishian (5), Steven A Carr (5), Aviv Regev (2,5,8)*#,, George M Church (1, David R Walt (1,6,7). Identification of markers for the isolation of neuron-specific extracellular vesicles. *bioRxiv* 2024[DOI: 10.1101/2024.04.03.587267]

69. Fujiwara H, Hasegawa M, Dohmae N, Kawashima A, Masliah E, et al. α-Synuclein is phosphorylated in synucleinopathy lesions. *Nature Cell Biology* 2002;4:160-4.[PMID: 11813001 DOI: 10.1038/ncb748]

70. Ramalingam N, Jin SX, Moors TE, et al. Dynamic physiological α-synuclein S129 phosphorylation is driven by neuronal activity. *NPJ Parkinsons Dis* 2023;9:4.[PMID: 36646701 PMCID: PMC9842642 DOI: 10.1038/s41531-023-00444-w]

71. Peng C, Gathagan RJ, Covell DJ, et al. Cellular milieu imparts distinct pathological α-synuclein strains in α-synucleinopathies. *Nature* 2018;557:558-63.[PMID: 29743672 PMCID: PMC5970994 DOI: 10.1038/s41586-018-0104-4]

72. Gibbons CH, Levine T, Adler C, et al. Skin Biopsy Detection of Phosphorylated α-Synuclein in Patients With Synucleinopathies. *JAMA* 2024;331:1298-306.[PMID: 38506839 PMCID: PMC10955354 DOI: 10.1001/jama.2024.0792]

73. Dutta S, Hornung S, Taha HB, et al. Development of a Novel Electrochemiluminescence ELISA for Quantification of α-Synuclein Phosphorylated at Ser(129) in Biological Samples. *ACS Chem Neurosci* 2023;14:1238-48.[PMID: 36920792 PMCID: PMC10080651 DOI: 10.1021/acschemneuro.2c00676]

74. Fauvet B, Lashuel HA. Semisynthesis and Enzymatic Preparation of Post-translationally Modified α-Synuclein. *Methods Mol Biol* 2016;1345:3-20.[PMID: 26453202 DOI: 10.1007/978-1-4939-2978-8_1]

75. Sasaki A, Arawaka S, Sato H, Kato T. Sensitive western blotting for detection of endogenous Ser129-phosphorylated α-synuclein in intracellular and extracellular spaces. *Sci Rep* 2015;5:14211.[PMID: 26381815 PMCID: PMC4585644 DOI: 10.1038/srep14211]

76. Herrera-Vaquero M, Bouquio D, et al. The molecular tweezer CLR01 reduces aggregated, pathologic, and seeding-competent α-synuclein in experimental multiple system atrophy. *Biochim Biophys Acta Mol Basis Dis* 2019;1865:165513.[PMID: 31319154 PMCID: PMC8425273 DOI: 10.1016/j.bbadis.2019.07.007]

77. Palma JA, Martinez J, Millar Vernetti P, et al. mTOR Inhibition with Sirolimus in Multiple System Atrophy: A Randomized, Double-Blind, Placebo-Controlled Futility Trial and 1-Year Biomarker Longitudinal Analysis. *Mov Disord* 2022;37:778-89.[PMID: 35040506 PMCID: PMC9018525 DOI: 10.1002/mds.28923]

78. Taha HB, Hornung S, Dutta S, et al. Toward a biomarker panel measured in CNS-originating extracellular vesicles for improved differential diagnosis of Parkinson's disease and multiple system atrophy. *Transl Neurodegener* 2023;12:14.[PMID: 36935518 PMCID: PMC10026428 DOI: 10.1186/s40035-023-00346-0]

79. Gomes DE, Witwer KW. L1CAM-associated extracellular vesicles: A systematic review of nomenclature, sources, separation, and characterization. *J Extracell Biol* 2022;1.[PMID: 35492832 PMCID: PMC9045013 DOI: 10.1002/jex2.35]

80. Tian C, Stewart T, Hong Z, et al. Blood extracellular vesicles carrying synaptic function- and brain-related proteins as potential biomarkers for Alzheimer's disease. *Alzheimers Dement* 2023;19:909-23.[PMID: 35779041 PMCID: PMC9806186 DOI: 10.1002/alz.12723]